THE JOURNAL OF BIOLOGICAL CHEMISTRY VOL. 287, NO. 10, pp. 7594–7602, March 2, 2012

Allosteric Modulation of Ca^{2+} flux in Ligand-gated Cation Channel (P2X4) by Actions on Lateral Portals*[S]

Received for publication, November 9, 2011, and in revised form, January 3, 2012 Published, JBC Papers in Press, January 4, 2012, DOI 10.1074/jbc.M111.322461

Damien S. K. Samways[‡1], **Baljit S. Khakh**[§], **and Terrance M. Egan**[‡2]

From the [‡]*Department of Pharmacological and Physiological Science and The Center for Excellence in Neuroscience, Saint Louis University School of Medicine, St. Louis, Missouri, 63130 and the* [§]*Departments of Physiology and Neurobiology, UCLA, David Geffen School of Medicine, Los Angeles, California 90095*

Background: Ca^{2+} currents of ligand-gated ion channels are essential to cell signaling.
Results: We show that the Ca^{2+} currents of P2X4 channels are subject to allosteric modulation.
Conclusion: The fixed negative charge of a single amino acid is required for the allosteric effects of ivermectin on permeability, flux, and current deactivation.
Significance: Allosteric modulators may provide therapeutic relief from symptoms of diseases such as peripheral neuropathy and hypertension.

Human P2X receptors are a family of seven ATP-gated ion channels that transport Na^+, K^+, and Ca^{2+} across cell surface membranes. The P2X4 receptor is unique among family members in its sensitivity to the macrocyclic lactone, ivermectin, which allosterically modulates both ion conduction and channel gating. In this paper we show that removing the fixed negative charge of a single acidic amino acid (Glu^{51}) in the lateral entrance to the transmembrane pore markedly attenuates the effect of ivermectin on Ca^{2+} current and channel gating. Ca^{2+} entry through P2X4 receptors is known to trigger downstream signaling pathways in microglia. Our experiments show that the lateral portals could present a novel target for drugs in the treatment of microglia-associated disease including neuropathic pain.

The Ca^{2+} currents of ligand-gated ion channels (LGICs)[3] play essential roles in cell signaling by regulating transmitter release, muscle contraction, and gene transcription (1, 2). Most cells are exquisitely sensitive to $[Ca^{2+}]_i$, and thus small changes in the amplitude of ligand-gated Ca^{2+} currents can lead to dramatic effects on the regulation of downstream Ca^{2+}-dependent signaling processes (3).

Recent works suggest that the ability to transport Ca^{2+} is not necessarily a fixed channel property of LGICs. This was first demonstrated in hippocampal neurons where PKA-dependent phosphorylation enhances NMDA-gated Ca^{2+} influx in dendritic spines by altering relative Ca^{2+} permeability, leading to facilitation of long term potentiation (4). Other notable recent examples include PKC-dependent modulation of the Ca^{2+} permeability of polymodal TRPV1 receptors (5) and agonist-dependent modulation of the Ca^{2+} currents of TRPV1 (6) and TRPA1 receptors (7) receptors.

Despite these examples, a central unanswered question is whether the Ca^{2+} currents of LGICs are susceptible to allosteric tuning by drugs (8). If this were so, then what is currently an interesting physiological phenomenon could be exploited pharmacologically. Thus, it might be possible to design drugs that allow channels to gate in response to their natural agonists but that alter the Ca^{2+} flux of the conducted currents in a way that influences downstream cellular processes.

Here we report that the macrocyclic lactone, ivermectin (IVM), reduces fractional Ca^{2+} current (*Pf*%) and relative Ca^{2+} permeability (P_{Ca}/P_{Cs}) through native and recombinant P2X4 receptor-channels, thus demonstrating for the first time allosteric modulation of the Ca^{2+} current of a LGIC by an exogenously applied drug. This effect is absent in mutant human P2X4 receptors (hP2X4Rs) that lack the fixed negative charge of a specific acidic amino acid (Glu^{51}) in the lateral entrance to the transmembrane pore (9, 10) and thereby identify a unique domain that might serve as a potential target for novel therapeutic agents.

EXPERIMENTAL PROCEDURES

Cell Culture of Mouse Cerebellar Microglia—Immortalized microglial C8-B4 cells were cultured in 35-mm dishes using Dulbecco's modified Eagle's medium (DMEM; Life Technologies, Grand Island, NY) supplemented with 10% fetal bovine serum (American Type Culture Collection, Manassas, VA), 2 mM glutamine, and antibiotics as previously described (11). The night before an experiment we added 1 μg/ml lipopolysaccharide (LPS) to the culture medium and incubated the cells for an additional 12 h. On the morning of the experiment the cells were dispersed using a trypsin/EDTA (1×) Hanks' buffered saline solution (Sigma), washed with DMEM, and replated onto polylysine-coated glass coverslips (Gold Seal; BD Biosciences) and bathed in a solution of DMEM and LPS. Electrophysiologi-

* This work was supported, in whole or in part, by National Institutes of Health Grants HL56236 (to T. M. E.) and NS073980 (to B. S. K.).
[S] This article contains supplemental Fig. 1.
[1] Present address: Dept. of Biology, 177 Science Center, Box 5805, Clarkson University, Potsdam, NY 13699-5805.
[2] To whom correspondence should be addressed: Dept. of Pharmacological and Physiological Science, Saint Louis University School of Medicine, 1402 South Grand Blvd., St. Louis, Missouri, 63104. Tel.: 314-977-6429; Fax: 314-977-6411; E-mail: egantm@slu.edu.
[3] The abbreviations used are: LGIC, ligand-gated ion channel; IVM, ivermectin; Pf%, fractional calcium current; P_{Ca}/P_{Cs}, relative calcium permeability; hP2X4R, human P2X4 receptor; LPS, lipopolysaccharide; mP2X4R, mouse P2X4 receptor; zfP2X4.1R, zebrafish P2X4.1 receptor.

cal recordings began 2–6 h later. We saw no ATP-gated currents in C8-B4 cells that were not exposed to LPS (11).

Mutagenesis—We studied recombinant hP2X4Rs that were made and expressed using conventional methods. Point mutations were engineered using the QuikChange Lightening Site-Directed Mutagenesis Kit (Stratagene, La Jolla, CA) and verified by automated DNA sequencing (Retrogen, San Diego, CA). Plasmid cDNA was delivered to cultured HEK293 cells using Lipofectamine LTX (Life Technologies).

Data Acquisition and Drug Application—Whole-cell currents were recorded with low resistance (1–3 megaohms), borosilicate glass pipettes (World Precision Instruments, Sarasota, FL), and AxoPatch 200B amplifiers (Molecular Devices, Sunnyvale, CA). Fura-2 fluorescence (510 nm excitation; 380 nm emission) was captured by a photomultiplier detection system (Photon Technology International, South Brunswick, NJ). Data were digitized at 10 kHz with Instrutech ITC-16 acquisition hardware (HEKA Instruments, Bellmore, NY) and AxoGraphX software (AxoGraph Scientific, Sydney, Australia). The stored data were analyzed off-line using AxoGraphX and Igor Pro software (WaveMetrics, Lake Oswego, OR). Fast solutions changes were achieved using a SF-77B Perfusion Fast-Step system (Warner Instruments, Hamden, CT). The concentration of IVM was 3 μM for amplitude and deactivation experiments and 10 μM for *Pf*% experiments except where otherwise noted.

Patch Clamp Photometry—The fraction of the total agonist-gated current carried by Ca^{2+} (*i.e. Pf*%) was measured using the dye-overload method of Neher (12) and Dani and co-workers (13). Our technique is described elsewhere in detail (14, 15). In short, HEK293 cells transiently expressing P2X receptors were grown in 35-mm culture dishes and then re-plated at low density onto poly-L-lysine-coated glass coverslips (Gold Seal) 2–3 h before the start of the experiment. Whole-cell current and fluorescence were recorded from adherent cells using a recording pipette containing 140 mM CsCl, 10 mM tetraethylammonium chloride, 3 mM CsOH, 10 mM HEPES, and 2 mM K_5-fura-2 at pH 7.3 (CsOH). The extracellular buffer contained 140 mM NaCl, 2 mM $CaCl_2$, 1 mM $MgCl_2$, 10 mM glucose, and 10 mM HEPES at pH 7.4 (NaOH). *Pf*% was determined from Equation 1,

$$Pf\% = \frac{Q_{Ca}}{Q_T} \times 100 \qquad \text{(Eq. 1)}$$

Q_{Ca} (in nC) equals $\Delta F_{380}/F_{max}$, ΔF_{380} is the change in fura-2 fluorescence caused by Ca^{2+} entry (measured in "bead units"), and F_{max} is a proportionality constant determined in separate sets of experiments (equal to 23.68 bead units/nC in most experiments). One bead units equals the average fluorescence of five Fluoresbrite 4.5 μM microspheres (Polysciences, Warrington, PA). Q_T is the total integrated agonist-gated current recorded using patch clamp electrophysiology (in nanocoulomb).

Bi-ionic Reversal Potential Measurements—We used round cells that were detached from cultures dishes by mechanical dispersion to minimize space-clamp errors. Whole-cell membrane current was recorded using indifferent electrodes suspended in 3 M KCl agar bridges in contact with the bath solution and the broken patch configuration of the whole-cell voltage clamp technique. The solution in the recording pipette was 150 mM CsCl, 10 mM EGTA, 10 mM HEPES, and pH 7.3 (CsOH). Relative Ca^{2+} permeability (P_{Ca}/P_{Cs}) was determined from the measured shift in reversal potential observed upon switching from the CsCl-based control solution to one composed of 110 mM $CaCl_2$, 10 mM glucose, 10 mM HEPES, 2 mM $CaOH_2$ (pH 7.4). We changed the membrane voltage of cells bathed in each solution from −80 to 60 mV at a constant rate (1.4 V/s) before and during agonist application, and we measured the zero current level (E_{Rev}) from the leak-subtracted currents. Then, P_{Ca}/P_{Cs} was determined as

$$\frac{P_{Ca}}{P_{Cs}} = \frac{(\gamma_{Ca}[Cs]_i) * \exp(\Delta E_{rev}F/RT) * (1 + \exp(\Delta E_{rev}F/RT))}{4\gamma_{Ca}[Ca]_o} \qquad \text{(Eq. 2)}$$

where ΔE_{rev} equals $E_{rev,Ca}$ minus $E_{rev,Cs}$ (16). The γ_{Cs} and γ_{Ca} represent the activity coefficients for Cs^+ (0.72 for 154 mM) and Ca^{2+} (0.26 for 112 mM), respectively.

Homology Model—We used the hP2X4R model built by Sébastien Dutertre (University of Queensland, St. Lucia, Australia) and based on the crystal structure of the zebrafish P2X4.1 receptor (zfP2X4.1R) (10) as previously described (9).

Statistical Tests and Reports—All data are presented as the mean ± S.E. of at least six experiments. Drug treatments were analyzed by comparing data obtained before and during drug treatment using the Student's *t* test function. Groups of data were analyzed by one-way analysis of variance with significance determined from the Tukey's protected multiple comparison test using Instat (GraphPad Software, La Jolla, CA). A $p \leq 0.01$ was considered significant.

RESULTS

IVM Reduces the Contribution of Ca^{2+} to ATP-gated Current of Mouse Cerebellar Microglia—The phenotypes of native homomeric P2X receptors are difficult to characterize because most tissues express more than one homologue and heteromeric receptors are common. We took advantage of the recent discovery of a pure population of mouse P2X4 receptors (mP2X4Rs) in LPS-stimulated C8-B4 microglia to study regulation of the Ca^{2+} current of a native ATP-gated ion channel (11). IVM is a positive allosteric modulator of rat (17) and human (18) P2X4 receptors. In recombinant hP2X4Rs, low concentrations ($EC_{50} \approx 0.3$ μM) of IVM increase the maximum current evoked by saturating concentrations of ATP, and at higher concentrations ($EC_{50} \approx 2$ μM), IVM also slows deactivation (18). Both of these effects are readily apparent in the native mP2X4R of activated C8-B4 cells (11). To determine the effect of IVM on *Pf*%, we applied ATP (100 μM, 3 s) while simultaneously measuring whole-cell current and fura-2 fluorescence. We found that the ATP-gated inward current (Fig. 1*A*) was accompanied by a decrease in the fluorescence intensity emitted at 510 nm by fura-2 when excited by 380 nm light, indicative of rise in the intracellular $[Ca^{2+}]_i$ (Fig. 1*B*). From these data, we calculated the *Pf*% of the mP2X4R to be 15.4 ± 1.2% (Table 1), as expected from previous results (11). Next, we bathed the cells in 10 μM IVM for 5 min and then reapplied ATP. The ATP-

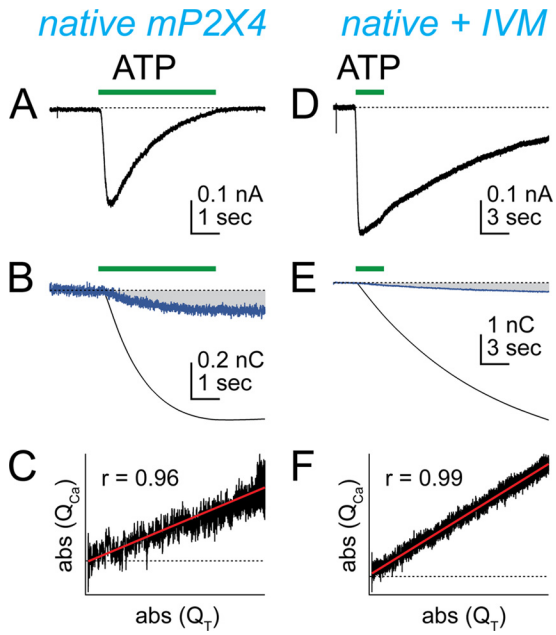

FIGURE 1. **IVM reduces the *Pf*% of C8-B4 microglia.** ATP-gated whole-cell current was recorded from mP2X4Rs of C8-B4 cells using patch pipettes containing the Ca^{2+}-sensitive dye, fura-2. ATP (100 μM) evoked an inward current (*A*) and a change in F_{380} (*B*, *blue trace*). Q_T (*B*, *black trace*) was determined by integrating the ATP-gated whole-cell current. The contribution of Q_{Ca} to Q_T is marked by the gray-shaded area of *panel B*. *Panel C* shows that Q_{Ca} is a linear function of Q_T. *Panels D*, *E*, and *F* show similar data obtained after a 5-min application of IVM (10 μM). IVM increased peak current amplitude and prolonged deactivation (*D*) and at the same time decreased *Pf*% (*E*). The decrease in *Pf*% was not caused by saturation of fura-2 because Q_{Ca} remained a linear function of Q_T (*F*).

TABLE 1

Effect of IVM on *Pf*%

Asterisks denote a significant difference between *Pf*% measured in the absence (i.e. control) and presence of 10 μM IVM. The number of trials for each experiment is indicated in parentheses.

Protein	Control	IVM
	%	%
mP2X4R (C8-B4 cells)	15.4 ± 1.2 (5)	7.0 ± 0.7 (6)*
rP2X1R	11.7 ± 0.6 (3)	10.0 ± 0.9 (3)
rP2X2R	7.3 ± 0.3 (10)	7.4 ± 0.6 (4)
hP2X4R	14.0 ± 0.7 (22)	8.1 ± 0.4 (14)*
hP2X4R-Y42W	17.5 ± 1.7 (7)	11.5 ± 1.8 (5)*
hP2X4R-V43W	13.9 ± 0.7 (5)	9.7 ± 0.9 (6)*
hP2X4R-E51Q	11.8 ± 0.3 (7)	9.9 ± 0.4 (6)
hP2X4R-D331N	11.3 ± 0.9 (5)	4.33 ± 0.7 (5)*
hP2X4R-E51Q/D331N	7.6 ± 0.9 (8)	7.0 ± 1.0 (6)
zfP2X4.1R	7.2 ± 1.3 (5)	6.7 ± 1.1 (7)
zfP2X4.1R-N54E/N334D	6.3 ± 0.8 (8)	5.3 ± 0.5 (11)

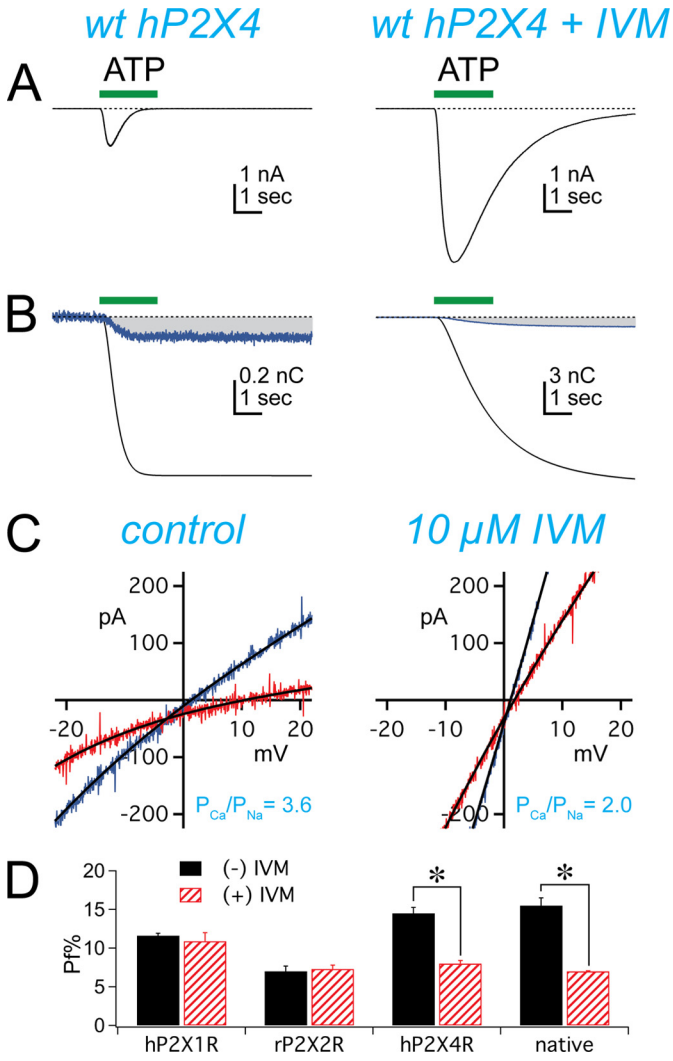

FIGURE 2. **IVM reduces the *Pf*% *of* recombinant hP2X4Rs.** Whole-cell currents were recorded from HEK293 cells using electrodes containing fura-2. ATP (30 μM) evoked inward currents (*A*) and changes in fura-2 fluorescence (*B*) in the absence (*left traces*) and presence (*right traces*) of IVM (10 μM). *Panel C* shows the effect of IVM on P_{Ca}/P_{Na}. Whole-cell current was recorded during voltage ramps to HEK293 cells expressing hP2X4Rs in the absence (*left panel*) and presence (*right panel*) of 10 μM IVM. *Blue traces* were obtained in high Na^+ extracellular solutions. *Red traces* were obtained in high Ca^{2+} extracellular solutions. The *solid black lines* are the polynomial fits to the raw data. *Panel D* shows the pooled data for the effect of IVM on the *Pf*% of P2XRs. IVM decreased the *Pf*% of native and recombinant P2X4Rs but had no effect on hP2X1Rs or rP2X2Rs.

gated current was larger in the presence of IVM, and deactivation was slower (Fig. 1*D*). We again calculated the *Pf*% from the change in fluorescence (Fig. 1*E*) and found that the *Pf*% was significantly smaller (7.0 ± 0.7%) than control (Table 1). The decrease in *Pf*% was not due to dye saturation because the calibrated change in fluorescence (*i.e.* the Q_{Ca}) was a linear function of the total charge transfer across the surface membrane (*i.e.* the Q_T) (Fig. 1, *C* and *F*). Moreover, these linear functions show that the rise in free $[Ca^{2+}]_i$ results solely from Ca^{2+} entry through the mP2X4R pore (19). To the best of our knowledge, this is the first report of allosteric modulation of the Ca^{2+} current of a native LGIC.

IVM Also Decreases Pf% of Recombinant hP2X4Rs—Next, we used the wild-type recombinant hP2X4R to determine whether the inhibition of *Pf*% we saw in mouse cells was independent of tissue and conserved across species. Using recombinant receptors also allowed us to exploit site-directed mutagenesis to study the molecular basis of the IVM effect. In keeping with published results (9, 14, 15), we found that the *Pf*% of the hP2X4R equaled 14.0 ± 0.7% in control conditions and was not significantly different from that measured from mP2X4Rs (Table 1). We also found that IVM had predictable effects (18); the ATP-gated currents of the hP2X4R evoked in the presence of 10 μM IVM were larger than control and deactivated slower (Fig. 2*A*). More importantly, we recapitulated the effect of IVM on the *Pf*% of native mP2X4Rs in the recombinant hP2X4Rs. That is, the *Pf*% of the ATP-gated current of the hP2X4R fell to 8.1 ± 0.4% in the presence of IVM (Fig. 2*B*). IVM also reduced

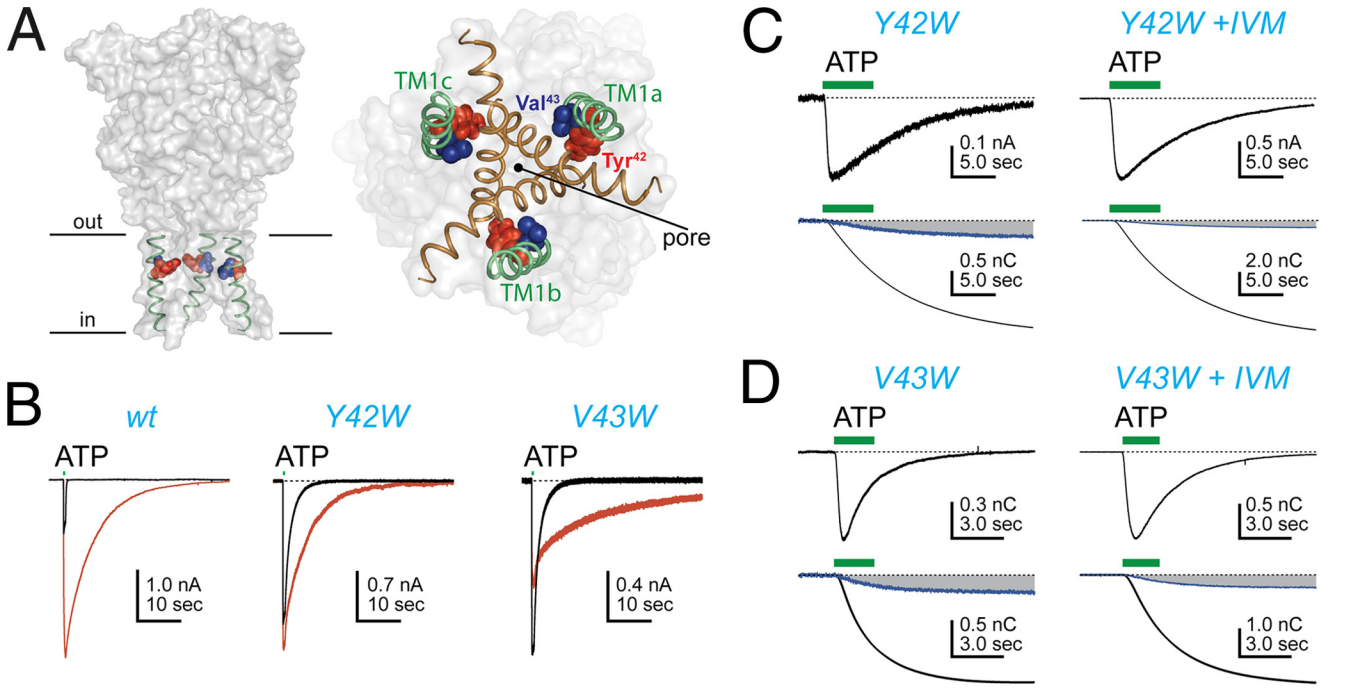

FIGURE 3. **Site-directed mutagenesis of TM1.** *Panel A* shows the location of Tyr^{42} (*red spheres*) and Val^{43} (*blue spheres*) along TM1 (*green*) in a homology model of the hP2X4R. The *left schematic* shows the channel viewed parallel to the membrane. The inner and outer limits of the membrane are marked with *lines*. The *right schematic* shows the protein viewed parallel to the 3-fold axis of symmetry from the intracellular side of the membrane. TM1 (*green*) lies lateral to TM2 (*brown*) and the pore. *Panel B* shows the effect of IVM (3 μM) on the ATP-gated (3 μM) currents of the wt and mutant receptors. *Panels C* and *D* show ATP-gated (30 μM) current and fluorescence traces recorded in the presence and absence of 10 μM IVM. These mutations had no significant effect on *Pf*% by comparison to the wt hP2X4R and no significant effect on the ability of IVM to reduce the *Pf*% (see Table 1).

the P_{Ca}/P_{Cs} of the hP2X4R, measured from the change in reversal potential of ATP-gated currents obtained in extracellular solutions containing predominately Na^+ or Ca^{2+} (Fig. 2*C*). P_{Ca}/P_{Cs} decreased from a control value of 4.3 ± 0.6 (n = 8) to a new value of 2.1 ± 0.1 (n = 3) in the presence of IVM.

Finally, we saw no effect of IVM on the *Pf*% of ATP-gated currents measured from HEK293 cells expressing either human P2X1 (hP2X1R) or rat P2X2 (rP2X2R) receptors (Fig. 2*D*; see also Table 1). These experiments support the claim that the effects of IVM are limited to P2X4Rs (20, 21).

We attempted to rigorously determine the IC_{50} of IVM on the *Pf*% and P_{Ca}/P_{Cs} of the hP2X4R but were hindered by the low aqueous solubility of the lactone in water at concentrations of >10 μM. Nevertheless, the effect of IVM was concentration-dependent because 3 μM IVM had a significantly smaller effect on *Pf*% (11.1 ± 0.6%; n = 9) than that measured in the presence of 10 μM IVM (supplemental Fig. S1*A*). Lower concentrations of IVM (0.1, 1 μM) also appeared to have concentration-dependent effects (supplemental Fig. S1*B*), although the significance of these inhibitions was difficult to determine because of the limited range of attainable values of *Pf*% (~11–15%) measured in the presence of less than 3 μM IVM. Nevertheless, the data clearly show that a low (μM) affinity IVM binding site mediates the reduction in *Pf*% (18).

In the remaining experiments we used site-directed mutagenesis of the recombinant wild-type (wt) hP2X4Rs and measurements of deactivation and *Pf*% to identify residues involved in the actions of IVM. We focused our study on sites previously shown to affect either channel gating (18, 22, 23) or *Pf*% (15, 24).

Site-directed Mutagenesis of TM1 Has No Effect on Ability of IVM to Decrease Pf%—P2X receptors have two transmembrane-spanning domains, designated TM1 and TM2. TM2 lines the pore (25–28) and regulates both the permeability and conductance of the ATP-gated current (14, 29–32). In contrast, there are sparse data to support such a role for TM1 in cation permeability or conduction (24, 33, 34). One exception is the finding that the *Pf*% of the rP2X2R is significantly reduced when either of two sites in TM1 (Tyr^{43} and Phe^{44}) is mutated to a hydrophobic alanine (24); similar results were recently reported for rP2X3 receptors (35). Mutagenesis of the homologous residues (Tyr^{42} and Val^{43}; Fig. 3*A*) of the hP2X4R to tryptophan reduces IVM sensitivity (22, 36), and so we hypothesized that these residues might be important for the effect of IVM on *Pf*%. Therefore, we compared the three effects of IVM (potentiation of current, prolongation of deactivation, and reduction in *Pf*%) on the ATP-gated currents of the wt receptor and the tryptophan mutants (Fig. 3, *B–D*).

First, we found that tryptophan mutagenesis blunted the effect of IVM on the size of the hP2X4R, as expected from similar work using the rat P2X4 ortholog (36). The peak current amplitude of the wt hP2X4R measured in the presence of IVM (3 μM) was 4.2 ± 0.9-fold larger than control (Table 2). In contrast, IVM caused a smaller potentiation of the hP2X4-Y42W current (1.2 ± 0.1-fold change) and inhibited the hP2X4-V43W current (0.6 ± 0.1) (Fig. 3*B*; Table 2). Although these differences are significant, a firm conclusion cannot be drawn for the following reason. IVM increases the current amplitude of the wt hP2X4R primarily by increasing the open time/probability

TABLE 2

Effect of IVM on peak current and deactivation

Deactivation rates are the $t_{90-10\%}$ times measured from the falling phase of the ligand-gated current that occured upon washout of ATP. ATP was applied at a concentration of 100 μM for zebrafish experiments and at a concentration of 3 μM in all other experiments. The concentration of IVM was 3 μM. The number of trials for each experiment is indicated in parentheses.

Protein	-Fold change in peak current by IVM	Deactivation rate control	Deactivation rate IVM	-Fold change in deactivation
		s	*s*	
hP2X4R	4.2 ± 0.9 (15)	0.14 ± 0.01 (18)	17.4 ± 2.4 (14)	124.3
hP2X4R-Y42W	1.2 ± 0.1 (10)	7.9 ± 1.1 (17)	14.2 ± 2.7 (9)	1.8
hP2X4R-V43W	0.6 ± 0.1 (8)	3.0 ± 0.4 (9)	19 ± 3.3 (5)	6.3
hP2X4R-E51Q	2.4 ± 0.5 (8)	0.32 ± 0.03 (11)	3.9 ± 1.1 (7)	12.2
hP2X4R-D331S	6.9 ± 1.5 (5)	0.36 ± 0.05 (13)	27.6 ± 6.4 (5)	76.7
hP2X4R-E51Q/D331S	2.2 ± 0.4 (6)	0.13 ± 0.01 (11)	1.7 ± 0.4 (5)	13.1
zfP2X4R	8.7 ± 3.5 (5)	0.13 ± 0.05 (4)	0.6 ± 0.1 (4)	4.6
zfP2X4R-N54E/N334D	40.1 ± 11.0 (4)	0.4 ± 0.1 (4)	14.0 ± 2.5 (4)	35

of the channel (18). If so, then two reasons could explain the smaller effects of IVM on the TM1 mutants. First, the mutations could limit the ability of IVM to increase open time. Second, the open time of the tryptophan-substituted mutants could be significantly greater than that of the wt receptor, which would limit the ability of IVM to further increase P_o. In-depth kinetic studies of the single channel currents of wt and mutant receptors are needed to identify the underlying cause, and such studies are problematic because of the extensive run-down in channel activity that is an innate property of hP2X4Rs (9, 18). We did not pursue these single channel experiments here because the focus of the present study is the effect of IVM on *Pf*%.

Next, we quantified deactivation by measuring the length of time it took for the agonist-gated current to fall from 90 to 10% of its peak current amplitude after washout of ATP (called the $t_{90-10\%}$ time). We found that the -fold changes in the rates of deactivation of the mutant receptors were less pronounced in the presence of 3 μM IVM (Fig. 3*B*), largely because tryptophan mutagenesis itself prolonged deactivation in the absence of IVM (Table 2). However, the absolute rates of deactivation of the wt and mutant receptors measured in the presence of IVM were not significantly different (see Table 2).

Finally, we measured the *Pf*% of these mutants before and after 10 μM IVM (Fig. 3, *C* and *D*). We found that replacing Tyr^{42} or Val^{43} of the hP2X4R with tryptophan had no significant effect on the *Pf*% in the absence of IVM despite the fact that alanine mutagenesis at the homologous sites of the rP2X2R (Tyr^{43} and Phe^{44}) significantly reduced *Pf*% (24). We also found that these mutations had no effect on the ability of IVM to attenuate the *Pf*% of the tryptophan-substituted receptors (Table 1). We draw two conclusions from these data. First, the fact that mutagenesis of Tyr^{42} and Val^{43} has no effect on *Pf*% supports the hypothesis that TM1 makes a smaller contribution to permeation than gating (24, 35, 37, 38). Second, Tyr^{42} and Val^{43} are not involved in the reduction of the *Pf*% of hP2X4Rs by IVM.

The Ability of IVM to Decrease Pf% Is Attenuated by Removing Fixed Negative Charge of Lateral Portals—The *Pf*% values of P2X1 and P2X4 receptors are approximately twice that of all other family members (14), in part because two acidic amino acids (Glu^{51} and Asp^{331} of the hP2X4R) provide an electrostatic environment that interacts with Ca^{2+} (15). In our homology model of the hP2X4R, Glu^{51} and Asp^{331} lie just extracellular to the transmembrane domains and form part of the lateral portals that are the extracellular entrance to the pore (9) (Fig. 4*A*). IVM affects P2X4 currents by intercalating with the transmembrane domains (36), an interaction that affects the accessibility of engineered cysteines of the lateral portals to water-soluble thiol-reactive compounds (9). Thus, we hypothesized that IVM may reduce *Pf*% by changing the topology of the lateral portals in a way that lowers the capacity of Glu^{51} and Asp^{331} to facilitate Ca^{2+} flux.

To test this hypothesis we investigated the IVM sensitivity of the hP2X4R mutants in which one or both of these acidic residues was replaced by the neutral amino acids that occupy the homologous positions (Gln^{52}, Ser^{326}) in the IVM-insensitive rP2X2R. In the first set of experiments, we measured the *Pf*% of the mutant hP2X4Rs in the absence of IVM. Consistent with published results (15), removing the single charge of either Glu^{51} (E51Q) or Asp^{331} (D331S) had no effect on *Pf*% (Table 1), whereas removing both charges (E51Q/D331S) significantly reduced *Pf*% to 7.6 ± 0.9%. After that, we measured the effect of 10 μM IVM on the *Pf*% of the three mutant receptors and found that the D331S mutant resembled the wild-type receptor because both showed equivalent reductions in *Pf*% in the presence of IVM (Fig. 4, *B* and *C*). In contrast, IVM failed to reduce the *Pf*% of either the E51Q (Fig. 4*D*) or the E51Q/D331S mutants (Fig. 4*C*; Table 1), which shows that the ability of IVM to regulate *Pf*% is critically dependent on the presence of the fixed negative charge of Glu^{51} in hP2X4R.

Removing the Fixed Charge of Glu^{51} Also Attenuates Effect of IVM on Current Deactivation—We then looked to see if removing the charge of Glu^{51} and/or Asp^{331} changed the ability of IVM to prolong deactivation after washout of 3 μM ATP. We found that the $t_{90-10\%}$ of the E51Q/D331S mutant increased from a control value of 0.13 ± 0.01 s to new value of 1.7 ± 0.4 s in the presence of 3 μM IVM. Although the prolongation is significant, it is ~10-fold shorter than the ~125-fold change observed for the wt receptor (Table 2). The effect of IVM on the $t_{90-10\%}$ of the ATP-gated current mediated by the E51Q mutant was also attenuated 10-fold (Fig. 4*E*), increasing from a control value of 0.32 ± 0.03 s in the absence of IVM to 3.9 ± 1.1 s in the presence of IVM. In contrast, IVM caused an ~80-fold increase in the time course of deactivation of currents mediated by the D331S mutant as the $t_{90-10\%}$ increased from 0.36 ± 0.05 s to 27.6 ± 6.4 s (Fig. 4*E*; Table 2).

Removing the fixed charge of Glu^{51} also reduced the effect of 3 μM IVM on current amplitude (Table 2). Again, the reduced ability to potentiate current could reflect either a change in the

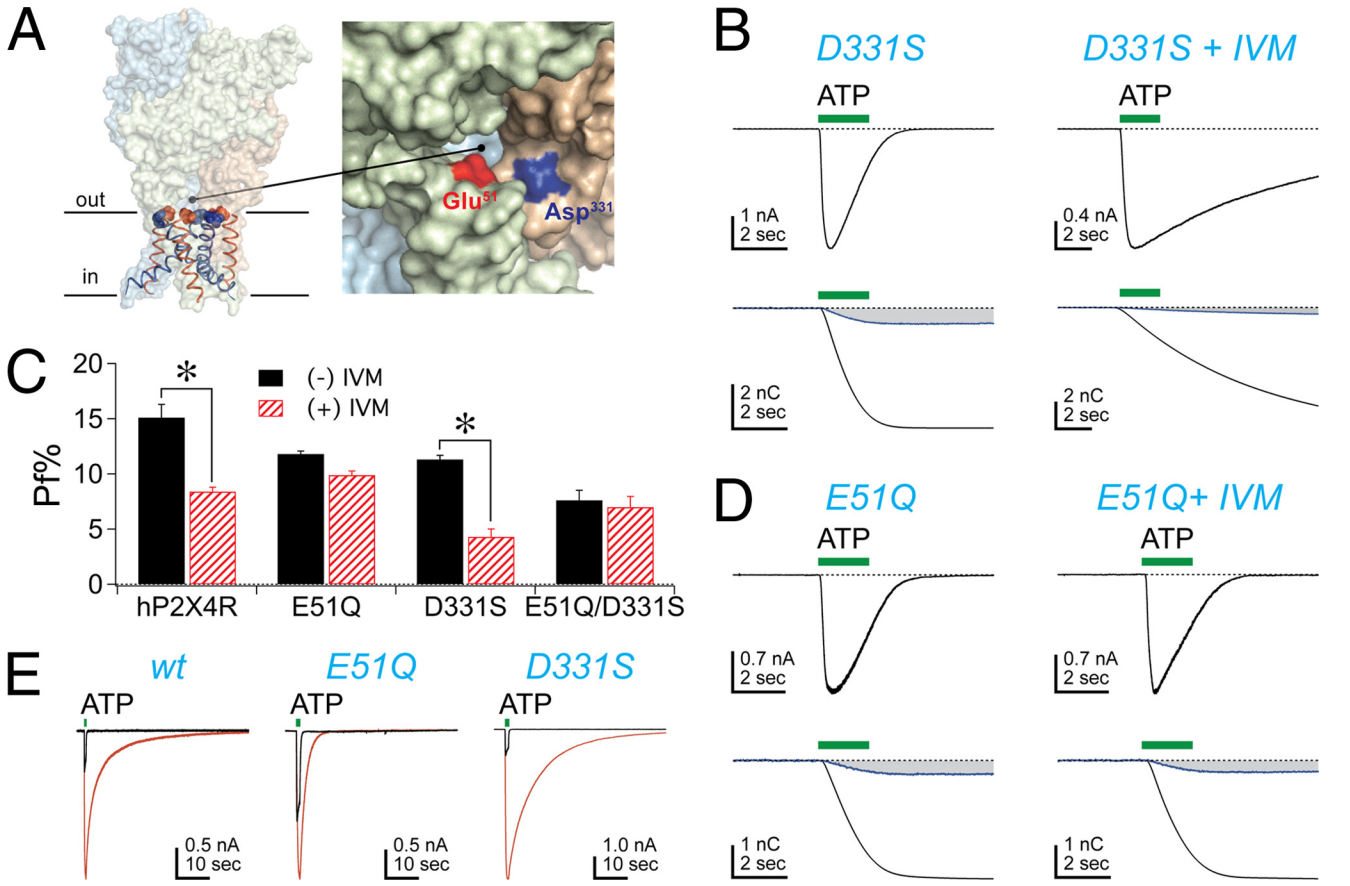

FIGURE 4. **Site-directed mutagenesis of the lateral portals.** *Panel A* shows the location of Glu^{51} (*red spheres*) and Asp^{331} (*blue spheres*) in our homology model of the hP2X4R. The *left schematic* shows the receptor viewed parallel to the membrane. The lateral portal is shown at a higher magnification in the *right schematic*. Here, the protein, as shown in the *left schematic*, is slanted 30° toward the viewer to give a view down into the portal entrance. *Panel B* shows ATP-gated (30 μM) current and fluorescence traces of D331S mutant receptors recorded from two different cells in the presence and absence of IVM (10 μM). In the *left traces*, the current was evoked in the absence of IVM. In the *right traces*, the cell was preincubated in IVM for 5 min before re-applying ATP. Currents evoked in the presence of IVM deactivated slower and had reduced *Pf*%. Average values of *Pf*% are shown in *Panel C*. *Panel D* shows ATP-gated current and fluorescence traces of two different cells expressing the E51Q mutant receptor evoked either in the absence (*left traces*) and presence (*right traces*) of IVM. *Panel E* shows the effect of 3 μM IVM on the kinetics of currents evoked by ATP (3 μM). Current was first tested in the absence of IVM (*black*). Then IVM was applied for 5 min, and ATP was reapplied to evoke modified current (*red*).

behavior of IVM or an innate property of the mutant channels as discussed above; we did not further investigate this effect.

Taken together, our data show that Glu^{51} is necessary for the effect of IVM on *Pf*% and current deactivation. The strong correlation of the effect of IVM on *Pf*% and deactivation suggests that a common final pathway may underlie both effects.

Substitution of Glu^{51} into zfP2X4.1R Imparts Limited Sensitivity to IVM—The zfP2X4.1R lacks the fixed negative charge of Glu^{51} and Asp^{331} and has a *Pf*% that is smaller than that of the hP2X4R (14, 15). Its sensitivity to IVM is unknown. We mutated the zfP2X4.1R to place acidic amino acids at sites equivalent to Glu^{51} and Asp^{331} of the hP2X4R and studied the effect of IVM on the wt and the double mutant (N34E/N334D) receptors. Our experiments produced four noteworthy results. First, in keeping with results obtained using other P2X4 orthologs (21), we found that 3 μM IVM caused a ~9-fold change in the peak current amplitude of the wt zfP2X4.1R caused by applying 100 μM ATP (Fig. 5*A*). To the best of our knowledge this is the first report of an effect of IVM on the zebrafish ortholog. Second, unlike its effects on the P2X4Rs of other species, IVM had no significant effect on the time course of current deactivation of the wt zfP2X4.1R (Fig. 5*A*). However, IVM substantially prolonged deactivation of the N54E/N334D double charge mutant (Fig. 5*B*), as the $t_{90-10\%}$ changed from a control value of 0.4 ± 0.1 s in control conditions to 14 ± 2.5 s in the presence of 3 μM IVM (Table 2). Again, in concordance with our results with the hP2X4R (see Fig. 4*E*), these data suggest that the effect of IVM on current deactivation requires the presence of a fixed charge in the lateral portal of P2X receptors. Third, inserting the fixed negative charges of glutamate and aspartate into the zfP2X4.1R had no effect on *Pf*% measured in the absence of IVM (Fig. 5*C*). This outcome was unexpected because the *Pf*% of the rP2X2R, which also lacks the two essential acidic amino acids, doubles after insertion of glutamate and aspartate at the equivalent sites (Fig. 5C (15)). Fourth, 10 μM IVM had no effect on the *Pf*% of currents evoked in cells expressing either the wt zfP2X4.1R or the zfP2X4.1-N54E/N334D double mutant (Fig. 5*C*). Why insertion of fixed charge failed to increase *Pf*% or impart IVM sensitivity to the *Pf*% of the zfP2X4.1R is presently unknown.

A Double Charge Mutant of rP2X2R Is IVM-insensitive—In a final set of experiments, we looked to see if we could impart full or limited sensitivity to IVM by inserting Glu^{51} into an IVM-insensitive, non-P2X4 receptor. The hP2X1R has an acidic

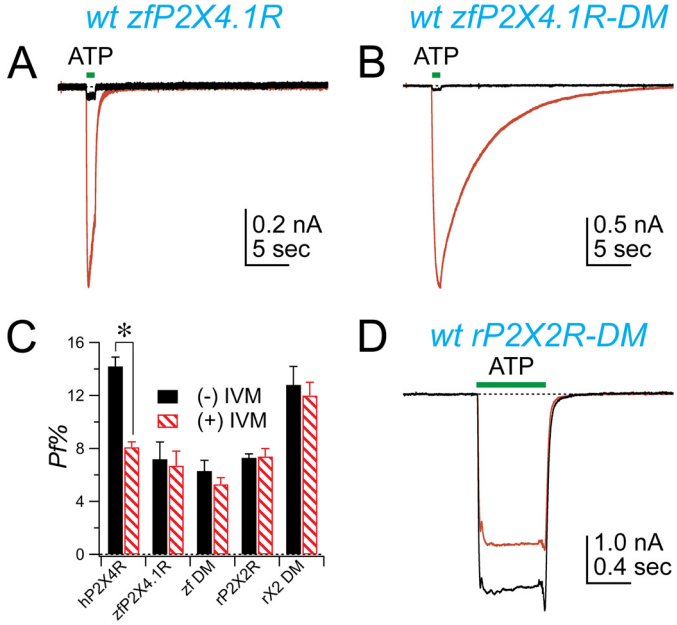

FIGURE 5. **Imparting IVM sensitivity through mutagenesis.** The figure shows the effect of IVM on wt and double mutant zfP2X4.1Rs. IVM (3 μM) increases peak amplitude of the ATP-gated (100 μM) current of the wt receptor without affecting the deactivation time course (*A*). The double mutant zfP2X4.1R showed an altered rate of deactivation in the presence of IVM (*B*). *Panel C* shows the pooled data. zfDM is the N54E/N334D double charge mutant of zfP2X4.1R; rX2 DM is the Q52E/S326D double charge mutant of rP2X2R. *Panel D* shows the lack of effect of IVM on the double mutant rP2X2R. ATP-gated currents were evoked in the absence (*black trace*) and presence (*red trace*) of IVM. The decrease in the peak current amplitude does not reflect an action of IVM because repeated ATP applications evoked in the absence of IVM show an identical decline (data not shown). The cause of the decline is unknown.

charge at the homologous site and a relatively high *Pf*% but is insensitive to the effects of IVM on *Pf*% (Fig. 2*D*), potentiation of current, and current deactivation. These data suggest that Glu^{51} is not the sole determinant of IVM sensitivity. To test this hypothesis, we measured the IVM sensitivity of a double rP2X2R mutant (Q52E/S326D) that contains fixed charge at sites equivalent to Glu^{51} and Asp^{331}. We found that current amplitude and the rate of deactivation of the double mutant rP2X2R-Q52E/S326D were not affected by IVM (Fig. 5*D*). The *Pf*% of rP2X2R-Q52E/S326D was similarly unaffected (Fig. 5*C*).

The following picture, therefore, emerges when all of the data are considered together. We conclude that the fixed negative charge of Glu^{51} is required for the slowed deactivation and reduced *Pf*% caused by the action of IVM on hP2X4Rs. However, Glu^{51} does not bestow IVM sensitivity by itself, as the effects of IVM sensitivity are restricted to P2X4Rs. The later finding suggests that additional structural loci unique to P2X4Rs are required for the multiple effects of IVM.

DISCUSSION

IVM has two well described effects on P2X4R current. First, it potentiates whole-cell current by binding to a high affinity (nM) site, and second, it prolongs deactivation by binding a low affinity (μM) site (17, 18, 39). In this report we show for the first time that IVM also reduces the contribution of Ca^{2+} to the ATP-gated current of native and recombinant P2X4Rs. Furthermore, the effects of IVM on deactivation and *Pf*% are markedly attenuated by removing the fixed negative charge of a single acidic amino acid (Glu^{51}) in the extracellular entrance to the transmembrane pore. Our finding that drugs modulate the ATP-gated Ca^{2+} current through actions on the lateral portals provide further support for the idea that these domains are flexible and move as the channel opens (9, 18). Drugs that alter these movements may, therefore, provide therapeutic relief from symptoms of diseases such as peripheral neuropathy (40) and hypertension (41).

Rather than point to a third and distinct action of IVM on P2X4R current, our data suggest that a common transduction pathway may underlie the effects of IVM on Ca^{2+} flux and current deactivation for the following two reasons. First, although the limited solubility of IVM in water prevented construction of a complete concentration-response curve, the available data suggest that IVM binds to a low affinity (μM) site to mediate its effect on *Pf*% (see supplemental Fig. S1). The micromolar potency of IVM at this site is similar to the estimated EC_{50} for the low affinity effect of IVM on deactivation. Second, removing the fixed negative charge of Glu^{51} substantially attenuates the effects of IVM on both *Pf*% and current deactivation, thus demonstrating a common structural locus in the lateral portals for both effects. Again, the lateral portals are flexible and move when the channel opens (9, 42). Our new data suggest that this movement may play a role in regulating the nature of cationic flux through the channel.

We speculate that the mechanism by which IVM attenuates *Pf*% and deactivation in P2X4Rs involves pushing the channel into a non-native conductance state with a lower P_{Ca}/P_{Na}. This hypothesis is partially supported by the single channel data of Priel and Silberberg (18) who showed that micromolar concentrations of IVM increase mean open time, open probability, and single channel conductance of the hP2X4R channel. The increase in conductance suggests that IVM decreases P_{Ca}/P_{Na} and *Pf*% by increasing Na^+ permeability and flux. Although this may be so, it cannot fully explain the magnitude of the effects described here. That is, a ~100% increase in the size of the Na^+ current is required to fully explain the observed 50% reduction in *Pf*% by IVM, which is far greater than the ~20% increase in single channel conductance reported by Priel and Silberberg (18). A concomitant decrease in Ca^{2+} permeability and flux is, therefore, required too.

Our data strongly suggest that Glu^{51} lies in a transduction pathway that mediates the low affinity effects of IVM. However, the data also imply that additional domains are involved in the selective effects of IVM on P2X4Rs. For example, the double mutant P2X2R (Q52E/S326D) has a glutamate at a position analogous to the Glu^{51} of P2X4R, but neither the *Pf*% nor the deactivation was altered by IVM. Similarly, wt hP2X1Rs have the equivalent charges but are unaffected by IVM. In contrast, the ability to prolong deactivation by IVM was successfully conferred to the zfP2X4R by introducing fixed charge at the position analogous to Glu^{51} of the hP2X4R. Interestingly, our data suggests that the wild-type zfP2X4R is still sensitive to the high affinity effects of IVM on current amplitude even though its deactivation lacks sensitivity to IVM. Further experiments comparing the zebrafish and mammalian P2X4R channels may help to tease apart the structural loci underpinning the separate

effects of IVM on channel function and explain why the effects are specific to P2X4R-like receptors.

Finally, we previously showed that the amplitude of the Ca^{2+} current of rat and human P2X1 and P2X4 receptors is highly dependent on the two relevant fixed charges of the lateral portals discussed here (15). The zfP2X4.1R lacks these acidic residues and has a lower *Pf*% than its mammalian counterparts. However, unlike our published results with rP2X2Rs (15), we did not record an increase in *Pf*% when carboxylates were added to the relevant positions in the zfP2X4.1R. We cannot fully explain the discrepancy between the double mutant rP2X2R and zfP2X4.1R results. Perhaps other undiscovered domains contribute to ion selection, and these domains are missing in the zfP2X4.1R. In addition, due to the low current densities achieved with maximal stimulation of these receptors in HEK293 cells (in the absence of IVM), we used long exposures to ATP (5–10 s) to obtain a Ca^{2+} flux that was large enough to accurately measure *Pf*%. These long applications may push the receptor into the I_2 permeability state (43), which may have different *Pf*% properties.

Acknowledgment—We thank Kelsey Eckelkamp for expert technical assistance.

REFERENCES

1. Burnashev, N. (1998) Calcium permeability of ligand-gated channels. *Cell Calcium* **24,** 325–332
2. Kisilevsky, A. E., and Zamponi, G. W. (2008) Presynaptic calcium channels: structure, regulators, and blockers. *Handb. Exp. Pharmacol.* **184,** 45–75
3. Berridge, M. J., Lipp, P., and Bootman, M. D. (2000) The versatility and universality of calcium signaling. *Nat. Rev. Mol. Cell Biol.* **1,** 11–21
4. Skeberdis, V. A., Chevaleyre, V., Lau, C. G., Goldberg, J. H., Pettit, D. L., Suadicani, S. O., Lin, Y., Bennett, M. V., Yuste, R., Castillo, P. E., and Zukin, R. S. (2006) Protein kinase A regulates calcium permeability of NMDA receptors. *Nat. Neurosci.* **9,** 501–510
5. Chung, M. K., Güler, A. D., and Caterina, M. J. (2008) TRPV1 shows dynamic ionic selectivity during agonist stimulation. *Nat. Neurosci.* **11,** 555–564
6. Samways, D. S., Khakh, B. S., and Egan, T. M. (2008) Tunable calcium current through TRPV1 receptor channels. *J. Biol. Chem.* **283,** 31274–31278
7. Karashima, Y., Prenen, J., Talavera, K., Janssens, A., Voets, T., and Nilius, B. (2010) Agonist-induced changes in Ca^{2+} permeation through the nociceptor cation channel TRPA1. *Biophys. J.* **98,** 773–783
8. Fesce, R., Forti, L., Polenghi, A., Locarno, A., Canella, R., Sacchi, O., and Rossi, M. L. (2011) Can selectivity be functionally modulated in ion channels? *J. Gen. Physiol.* **138,** 367–370
9. Samways, D. S., Khakh, B. S., Dutertre, S., and Egan, T. M. (2011) Preferential use of unobstructed lateral portals as the access route to the pore of human ATP-gated ion channels (P2X receptors). *Proc. Natl. Acad. Sci. U.S.A.* **108,** 13800–13805
10. Kawate, T., Michel, J. C., Birdsong, W. T., and Gouaux, E. (2009) Crystal structure of the ATP-gated P2X(4) ion channel in the closed state. *Nature* **460,** 592–598
11. Toulme, E., Garcia, A., Samways, D., Egan, T. M., Carson, M. J., and Khakh, B. S. (2010) P2X4 receptors in activated C8-B4 cells of cerebellar microglial origin. *J. Gen. Physiol.* **135,** 333–353
12. Neher, E. (1995) The use of fura-2 for estimating Ca^{2+} buffers and Ca^{2+} fluxes. *Neuropharmacology* **34,** 1423–1442
13. Vernino, S., Rogers, M., Radcliffe, K. A., and Dani, J. A. (1994) Quantitative measurement of calcium flux through muscle and neuronal nicotinic acetylcholine receptors. *J. Neurosci.* **14,** 5514–5524
14. Egan, T. M., and Khakh, B. S. (2004) Contribution of calcium ions to P2X channel responses. *J. Neurosci.* **24,** 3413–3420
15. Samways, D. S., and Egan, T. M. (2007) Acidic amino acids impart enhanced Ca^{2+} permeability and flux in two members of the ATP-gated P2X receptor family. *J. Gen. Physiol.* **129,** 245–256
16. Lewis, C. A. (1979) Ion concentration dependence of the reversal potential and the single channel conductance of ion channels at the frog neuromuscular junction. *J. Physiol.* **286,** 417–445
17. Khakh, B. S., Proctor, W. R., Dunwiddie, T. V., Labarca, C., and Lester, H. A. (1999) Allosteric control of gating and kinetics at P2X(4) receptor channels. *J. Neurosci.* **19,** 7289–7299
18. Priel, A., and Silberberg, S. D. (2004) Mechanism of ivermectin facilitation of human P2X4 receptor channels. *J. Gen. Physiol.* **123,** 281–293
19. Schneggenburger, R., Zhou, Z., Konnerth, A., and Neher, E. (1993) Fractional contribution of calcium to the cation current through glutamate receptor channels. *Neuron* **11,** 133–143
20. Jarvis, M. F., and Khakh, B. S. (2009) ATP-gated P2X cation channels. *Neuropharmacology* **56,** 208–215
21. Coddou, C., Yan, Z., Obsil, T., Huidobro-Toro, J. P., and Stojilkovic, S. S. (2011) Activation and regulation of purinergic P2X receptor channels. *Pharmacol. Rev.* **63,** 641–683
22. Jelínkova, I., Vávra, V., Jindrichova, M., Obsil, T., Zemkova, H. W., Zemkova, H., and Stojilkovic, S. S. (2008) Identification of P2X(4) receptor transmembrane residues contributing to channel gating and interaction with ivermectin. *Pflugers Arch.* **456,** 939–950
23. Jindrichova, M., Vavra, V., Obsil, T., Stojilkovic, S. S., and Zemkova, H. (2009) Functional relevance of aromatic residues in the first transmembrane domain of P2X receptors. *J. Neurochem.* **109,** 923–934
24. Samways, D. S., Migita, K., Li, Z., and Egan, T. M. (2008) On the role of the first transmembrane domain in cation permeability and flux of the ATP-gated P2X2 receptor. *J. Biol. Chem.* **283,** 5110–5117
25. Rassendren, F., Buell, G., Newbolt, A., North, R. A., and Surprenant, A. (1997) Identification of amino acid residues contributing to the pore of a P2X receptor. *EMBO J.* **16,** 3446–3454
26. Egan, T. M., Haines, W. R., and Voigt, M. M. (1998) A domain contributing to the ion channel of ATP-gated P2X2 receptors identified by the substituted cysteine accessibility method. *J. Neurosci.* **18,** 2350–2359
27. Li, M., Chang, T. H., Silberberg, S. D., and Swartz, K. J. (2008) Gating the pore of P2X receptor channels. *Nat. Neurosci.* **11,** 883–887
28. Kracun, S., Chaptal, V., Abramson, J., and Khakh, B. S. (2010) Gated access to the pore of a P2X receptor. Structural implications for closed-open transitions. *J. Biol. Chem.* **285,** 10110–10121
29. Nakazawa, K., Inoue, K., and Ohno, Y. (1998) An asparagine residue regulating conductance through P2X2 receptor/channels. *Eur. J. Pharmacol.* **347,** 141–144
30. Cao, L., Young, M. T., Broomhead, H. E., Fountain, S. J., and North, R. A. (2007) Thr-339-to-serine substitution in rat P2X2 receptor second transmembrane domain causes constitutive opening and indicates a gating role for Lys308. *J. Neurosci.* **27,** 12916–12923
31. Migita, K., Haines, W. R., Voigt, M. M., and Egan, T. M. (2001) Polar residues of the second transmembrane domain influence cation permeability of the ATP-gated P2X(2) receptor. *J. Biol. Chem.* **276,** 30934–30941
32. Browne, L. E., Cao, L., Broomhead, H. E., Bragg, L., Wilkinson, W. J., and North, R. A. (2011) P2X receptor channels show threefold symmetry in ionic charge selectivity and unitary conductance. *Nat. Neurosci.* **14,** 17–18
33. Haines, W. R., Voigt, M. M., Migita, K., Torres, G. E., and Egan, T. M. (2001) On the contribution of the first transmembrane domain to whole-cell current through an ATP-gated ionotropic P2X receptor. *J. Neurosci.* **21,** 5885–5892
34. Li, M., Kawate, T., Silberberg, S. D., and Swartz, K. J. (2010) Open for business. *Nat. Commun.* **1,** 1–7
35. Jindrichova, M., Khafizov, K., Skorinkin, A., Fayuk, D., Bart, G., Zemkova, H., and Giniatullin, R. (2011) Highly conserved tyrosine 37 stabilizes desensitized states and restricts calcium permeability of ATP-gated P2X3 receptor. *J. Neurochem.* **119,** 676–685
36. Silberberg, S. D., Li, M., and Swartz, K. J. (2007) Ivermectin interaction with transmembrane helices reveals widespread rearrangements during

opening of P2X receptor channels. *Neuron* **54,** 263–274
37. Haines, W. R., Migita, K., Cox, J. A., Egan, T. M., and Voigt, M. M. (2001) The first transmembrane domain of the P2X receptor subunit participates in the agonist-induced gating of the channel. *J. Biol. Chem.* **276,** 32793–32798
38. Keceli, B., and Kubo, Y. (2009) Functional and structural identification of amino acid residues of the P2X2 receptor channel critical for the voltage- and ATP-dependent gating. *J. Physiol.* **587,** 5801–5818
39. Jelínková, I., Yan, Z., Liang, Z., Moonat, S., Teisinger, J., Stojilkovic, S. S., and Zemková, H. (2006) Identification of P2X4 receptor-specific residues contributing to the ivermectin effects on channel deactivation. *Biochem. Biophys. Res. Commun.* **349,** 619–625
40. Tsuda, M., Shigemoto-Mogami, Y., Koizumi, S., Mizokoshi, A., Kohsaka, S., Salter, M. W., and Inoue, K. (2003) P2X4 receptors induced in spinal microglia gate tactile allodynia after nerve injury. *Nature* **424,** 778–783
41. Yamamoto, K., Sokabe, T., Matsumoto, T., Yoshimura, K., Shibata, M., Ohura, N., Fukuda, T., Sato, T., Sekine, K., Kato, S., Isshiki, M., Fujita, T., Kobayashi, M., Kawamura, K., Masuda, H., Kamiya, A., and Ando, J. (2006) Impaired flow-dependent control of vascular tone and remodeling in P2X4-deficient mice. *Nat. Med.* **12,** 133–137
42. Kawate, T., Robertson, J. L., Li, M., Silberberg, S. D., and Swartz, K. J. (2011) Ion access pathway to the transmembrane pore in P2X receptor channels. *J. Gen. Physiol.* **137,** 579–590
43. Khakh, B. S., Bao, X. R., Labarca, C., and Lester, H. A. (1999) Neuronal P2X transmitter-gated cation channels change their ion selectivity in seconds. *Nat. Neurosci.* **2,** 322–330